Research Square

Preprints are preliminary reports that have not undergone peer review.
They should not be considered conclusive, used to inform clinical practice,
or referenced by the media as validated information.

CYLD-associated K63-linked ubiquitin dysregulation contributes to synaptic and autism-related behavioral abnormalities after maternal thyroid hormone deficiency

Dijie Liu

liudijie@cmu.edu.cn

China Medical University https://orcid.org/0009-0006-0207-8495

Kai Tao

Shiyong Wang

Shu Liu

China Medical University

Ying Sun

Article

Keywords: Maternal thyroid hormone deficiency, autism-related behavior, CYLD, K63-linked ubiquitination, synaptic protein homeostasis, hippocampal development

Posted Date: October 21st, 2026

DOI: https://doi.org/10.21203/rs.3.rs-11009739/v1

License: This work is licensed under a Creative Commons Attribution 4.0 International License.
Read Full License

Additional Declarations: There is **NO** Competing Interest.

Abstract

Maternal thyroid hormone deficiency (MTHD) increases offspring neurodevelopmental risk, but the post-translational mechanisms underlying persistent synaptic dysfunction remain unclear. We investigated CYLD-associated ubiquitin dysregulation in a rat model established by thyroidectomy and low-dose L-thyroxine supplementation. Adolescent male offspring underwent behavioral testing, hippocampal histological examination, and molecular analyses. AAV9-mediated CYLD overexpression was performed bilaterally in the hippocampus on postnatal day 28. MTHD offspring exhibited impaired social interaction and novelty recognition, increased repetitive grooming and anxiety-like behavior, spatial learning and memory deficits, and hippocampal CA1 neuronal injury. These abnormalities were accompanied by reduced CYLD expression, increased high-molecular-weight K63-linked and Met1-linked ubiquitin signals, decreased PSD95, synaptophysin, Synapsin I, and GluA1 expression, and attenuated BDNF-CREB signaling. CYLD overexpression reduced K63-linked ubiquitin accumulation, partially restored PSD95, Synapsin I, and GluA1 expression, and improved social, anxiety-like, and cognitive outcomes. These findings implicate CYLD-associated K63-linked ubiquitin dysregulation in MTHD-induced hippocampal synaptic protein disturbances and identify a potentially modifiable pathway contributing to offspring neurodevelopmental impairment.

1. INTRODUCTION

Maternal thyroid hormones provide essential endocrine signals for early brain development by coordinating neurogenesis, neuronal migration, synaptogenesis, and circuit maturation [1, 2]. Before the fetal hypothalamic-pituitary-thyroid axis becomes functional, the developing brain depends substantially on maternal thyroid hormone supply. Maternal thyroid hormone deficiency (MTHD) is therefore a clinically relevant prenatal exposure associated with cognitive, attentional, and behavioral impairments and with increased risk of autism spectrum disorder and related neurodevelopmental outcomes in offspring [3]. Experimental studies further indicate that disrupted thyroid hormone signaling affects molecular programs required for neuronal and synaptic development. A central unresolved question is how gestational thyroid hormone deficiency becomes biologically embedded and produces persistent postnatal synaptic and behavioral phenotypes.

Most mechanistic studies of MTHD-related brain injury have focused on impaired neurogenesis, altered neuronal migration, reduced neurotrophic support, and lower synaptic protein abundance. These processes are important, but protein abundance alone does not explain how an early endocrine disturbance alters later circuit maturation. Developing synapses require coordinated control of protein assembly, localization, trafficking, turnover, and clearance [4, 5]. Disruption of this homeostatic layer during sensitive developmental periods can alter synaptic trajectories and contribute to persistent neurodevelopmental phenotypes [6, 7]. Defining the post-translational mechanisms that connect prenatal thyroid hormone deficiency to synaptic dysfunction may therefore clarify a molecular pathway relevant to autism-related behavior.

The ubiquitin system is a major post-translational network governing protein homeostasis and signaling [8, 9]. K63-linked ubiquitination primarily mediates non-degradative functions, including protein-complex assembly, membrane trafficking, cytoskeletal regulation, and signaling-platform formation [10, 11]. These processes are directly relevant to synaptic organization, receptor localization, and activity-dependent plasticity. CYLD is a deubiquitinase with strong activity toward K63-linked ubiquitin chains [12, 13]. Although CYLD has been implicated in neuronal morphogenesis and synaptic regulation, it remains unknown whether altered CYLD-dependent ubiquitin homeostasis connects gestational thyroid hormone deficiency to autism-related synaptic and behavioral abnormalities.

We tested the hypothesis that MTHD impairs offspring hippocampal development by disrupting CYLD-associated K63-linked ubiquitin homeostasis. Using a rat model, we assessed social interaction and novelty recognition, repetitive grooming, anxiety-like behavior, and hippocampus-dependent spatial learning and memory in adolescent male offspring. We then examined hippocampal structure, CYLD expression, K63-linked and linear ubiquitin signals, synapse-associated proteins, and BDNF-CREB signaling. Finally, we increased hippocampal CYLD expression after postnatal day 28 using AAV-CYLD to test whether restoring CYLD could attenuate ubiquitin imbalance, synaptic protein loss, and behavioral abnormalities. This design examined CYLD-associated ubiquitin homeostasis as a functional and potentially modifiable molecular pathway linking MTHD to autism-related neurodevelopmental phenotypes.

2. MATERIALS AND METHODS

2.1 Animals and Experimental Design

Adult female Wistar rats, 8–10 weeks of age and weighing 180–220 g, and adult male Wistar rats, weighing 250–300 g, were obtained from the Experimental Animal Center of China Medical University. All animals were housed in a specific pathogen-free facility under controlled conditions of 22 ± 2°C, 50%-60% relative humidity, and a 12 h light/dark cycle, with free access to food and water. All experimental procedures were conducted in accordance with the National Institutes of Health Guide for the Care and Use of Laboratory Animals and were approved by the Ethics Committee for Animal Experiments of China Medical University (Approval No. KT20242238).

In this study, a rat model of maternal thyroid hormone deficiency (MTHD) was used in combination with behavioral assessment, hippocampal histopathological examination, protein and gene expression analyses, and postnatal hippocampal AAV-CYLD intervention to evaluate the long-term effects of maternal thyroid hormone deficiency on offspring neurodevelopment and to investigate the relationship between CYLD-related synaptic homeostatic alterations and neurodevelopmental abnormalities. The overall experimental workflow is shown in Fig. 1. After recovery from sham surgery or thyroidectomy and confirmation of the maternal thyroid hormone deficiency model, female rats were mated with healthy males at a ratio of 2:1. The presence of a vaginal plug was checked the following morning, and the day on which a plug was detected was designated gestational day 0 (GD0). Pregnant dams were assigned to

the Control or MTHD group according to their pre-established surgical/modeling status. Dams in the Control group underwent sham surgery and maintained normal pregnancy, whereas dams in the MTHD group were used to establish and maintain maternal thyroid hormone deficiency throughout gestation. Maternal endocrine validation was performed at the dam level, with 15 dams analyzed per group. Within 24 h after birth, the number of pups per dam was standardized to nine to minimize differences in lactational nutrition. Only male offspring were included in subsequent experiments to avoid potential confounding effects of sex on neurodevelopmental outcomes. Offspring behavioral, histological, and molecular analyses were performed using male pups sampled from nine independent litters per group. For each experimental endpoint, one male offspring was taken from each litter, so no endpoint included more than one pup from the same litter as independent biological observations. Thus, the offspring sample size represents biologically independent litters/offspring rather than multiple pups drawn from fewer litters. During adolescence, offspring underwent behavioral testing, including the Open Field Test, Three-Chamber Social Test, and Morris Water Maze. After completion of behavioral assessments, animals were anesthetized and euthanized, and hippocampal tissues were rapidly dissected for histological analysis, Western blotting, real-time quantitative PCR (RT-qPCR), and related molecular assays.

2.2 Establishment of the Maternal Thyroid Hormone Deficiency Model and AAV-CYLD Intervention

Adult female Wistar rats, 8–10 weeks of age and weighing 180–220 g, were randomly assigned to the Control group or the maternal thyroid hormone deficiency (MTHD) group. All animals were acclimatized for 1 week before the experiments.

The MTHD model was established according to a previously developed and validated protocol from our laboratory [14]. Briefly, rats in the MTHD group underwent total thyroidectomy under anesthesia with 3% sodium pentobarbital (0.1 mL/100 g, intraperitoneally). During surgery, the parathyroid glands and recurrent laryngeal nerves were carefully preserved to minimize postoperative complications. Rats in the Control group underwent sham surgery, in which the thyroid gland was exposed but not removed. After surgery, penicillin was administered intramuscularly (40,000 U/rat) to prevent infection, and 0.1% (w/v) calcium lactate was added to the drinking water to prevent hypocalcemia related to potential parathyroid impairment. Animals were allowed to recover for 1 week after surgery.

After the recovery period, rats in the MTHD group received daily subcutaneous injections of low-dose L-thyroxine (L-T_4; Sigma-Aldrich, USA) at 0.5μg/100 g body weight to maintain a state of maternal thyroid hormone deficiency, characterized by elevated TSH and reduced TT_4 levels. After successful establishment of the model, female rats were mated with males at a male: female ratio of 1:2. Vaginal plugs were checked the next morning, and the day on which a plug was detected was defined as gestational day 0 (GD0). Pregnant rats were housed individually throughout gestation until spontaneous delivery. Maternal venous blood was collected on GD7, GD13, and postnatal day 1 (PND1) to measure serum total thyroxine (TT_4) and thyroid-stimulating hormone (TSH) levels and to assess model validity.

To further determine the role of CYLD in MTHD-induced behavioral and hippocampal synaptic abnormalities, male offspring received hippocampal AAV-CYLD intervention on postnatal day 28 (P28). Offspring rats were randomly assigned to the Control + AAV-GFP, MTHD + AAV-GFP, or MTHD + AAV-CYLD group. Recombinant AAV-CYLD and control AAV-GFP vectors were packaged in an AAV9 backbone under the control of the hSyn promoter and delivered at a final titer of 1.0 × 1012 vg/mL. Under isoflurane anesthesia, rats were fixed in a stereotaxic apparatus, and viruses were bilaterally injected into the hippocampus using coordinates relative to bregma: anteroposterior, − 3.6 mm; mediolateral, ± 2.2 mm; dorsoventral, − 3.2 mm. A total of 1.0 μL virus was infused per side at 0.1 μL/min. The needle was left in place for 5 min after infusion to minimize reflux before slow withdrawal. Animals recovered in a temperature-controlled environment and received routine postoperative care. CYLD overexpression in the hippocampus was verified by Western blotting before downstream analyses.

Approximately 3–4 weeks after AAV injection, offspring underwent behavioral testing at P50-P60, including the Three-Chamber Social Test, Open Field Test, and Morris Water Maze, to assess social behavior, anxiety-like behavior, and hippocampus-dependent spatial learning and memory. After behavioral testing, animals were euthanized and hippocampal tissues were rapidly dissected for Western blot analysis of CYLD, K63-linked ubiquitination, PSD95, Synapsin I, GluA1, and related markers, to evaluate the effects of AAV-CYLD intervention on behavioral outcomes, hippocampal ubiquitin homeostasis, and synaptic protein homeostasis in offspring.

2.3 Behavioral Assessment

All behavioral tests were performed in adolescent male offspring aged 5–8 weeks. During testing, the room was maintained at 22 ± 2°C and 50%-60% relative humidity, and experiments were conducted between 09:00 and 17:00 each day. Animals were allowed to acclimate to the testing room for 30 min before each test. After each trial, the apparatus was thoroughly cleaned with 75% ethanol to remove olfactory cues. All behavioral analyses were performed by investigators blinded to group allocation.

2.3.1 Three-Chamber Social Test

The three-chamber social test was used to assess social interaction and preference for social novelty in offspring rats [15]. The apparatus consisted of a transparent acrylic box (60 cm × 40 cm × 22 cm) divided into three equal chambers by two partitions, with small openings allowing free movement between chambers. Identical wire cages (10 cm in diameter, 12 cm in height) were placed in the left and right chambers.

The test consisted of three phases. In the habituation phase, the test rat was placed in the central chamber and allowed to freely explore the entire apparatus for 10 min. In the social interaction phase, an unfamiliar age- and sex-matched Wistar rat (Stranger 1) was placed inside the wire cage in one side chamber, while the opposite cage remained empty. The test rat was allowed to explore freely for 10 min, and the time spent interacting with Stranger 1 or the empty cage was recorded. In the social novelty phase, Stranger 1 remained in place, and a second unfamiliar rat (Stranger 2) was placed in the

previously empty cage. The test rat was allowed to explore for another 10 min, and the time spent interacting with the familiar rat (Stranger 1) and the novel rat (Stranger 2) was recorded.

Social contact was defined as active sniffing of the animal inside the wire cage with the nose positioned within approximately 2 cm of the cage. Time spent merely staying near, climbing on, or leaning against the wire cage was not counted as social contact. All videos were analyzed offline by investigators blinded to experimental grouping.

2.3.2 Open Field Test

The open field test was used to evaluate spontaneous locomotor activity, exploratory behavior, and anxiety-like behavior in offspring rats [16]. The apparatus consisted of a white opaque acrylic box (100 cm × 100 cm × 40 cm). The central 50 cm × 50 cm area was defined as the center zone, and the remaining area was defined as the peripheral zone.

At the beginning of the test, each rat was gently placed in the center of the arena and allowed to explore freely for 10 min. Behavior was continuously recorded by an overhead camera, and movement trajectories were automatically tracked using a video-tracking system (EthoVision XT, Noldus Information Technology, The Netherlands).

The analyzed parameters included total distance traveled, average velocity, time spent in the center zone, number of center entries, and rearing behavior. After each trial, the apparatus was thoroughly cleaned with 75% ethanol and allowed to dry to remove residual odors. Data analysis was performed by investigators blinded to group allocation.

2.3.3 Self-Grooming Test

The self-grooming test was used to assess repetitive stereotyped behavior in offspring rats [17]. Each rat was individually placed in a transparent acrylic box (40 cm × 30 cm × 30 cm) containing a small amount of fresh bedding. After a 10 min habituation period, behavior was recorded continuously for 10 min to assess spontaneous grooming.

Self-grooming was defined as continuous cleaning or grooming movements directed toward the face, head, ears, trunk, limbs, or tail using the forepaws or mouth. The total duration of self-grooming during the observation period was quantified. If grooming was interrupted by exploratory activity lasting more than 3 s, the subsequent grooming episode was considered a new event. All videos were analyzed offline by investigators blinded to group allocation. After each test, the apparatus was thoroughly cleaned with 75% ethanol to eliminate residual odors.

2.3.4 Morris Water Maze

The Morris Water Maze (MWM) was used to assess hippocampus-dependent spatial learning and memory in offspring rats [18]. The apparatus consisted of a circular pool 150 cm in diameter and 50 cm in height, filled with water maintained at 22 ± 1°C. A suitable amount of non-toxic white dye was added to

make the water opaque. A circular escape platform, 10 cm in diameter, was placed in the center of the target quadrant, with its top surface approximately 1.5 cm below the water surface. Extra-maze spatial cues were kept constant throughout the experiment.

The test consisted of an acquisition training phase and a probe trial. Acquisition training was conducted for 5 consecutive days, with four trials per day. In each trial, rats were released into the pool from one of four randomly selected starting points and allowed to search for the hidden platform for a maximum of 60 s. If a rat failed to locate the platform within 60 s, it was gently guided to the platform and allowed to remain there for 15 s to facilitate spatial memory formation.

Twenty-four hours after the final training session, the probe trial was conducted. The platform was removed, and each rat was released into the pool from a randomly selected starting point and allowed to swim freely for 60 s. Movement trajectories were recorded using EthoVision XT software (Noldus Information Technology, The Netherlands). Time spent in the target quadrant was used as the primary outcome measure to evaluate spatial memory retention. All data were analyzed by investigators blinded to experimental grouping.

2.4 Hippocampal Tissue Collection and Nissl Staining

After completion of behavioral testing, offspring rats were deeply anesthetized with 3% sodium pentobarbital (40 mg/kg, intraperitoneally). For histological analysis, animals were transcardially perfused with 0.9% saline followed by fixation with 4% paraformaldehyde (PFA). Whole brains were removed and post-fixed in 4% PFA at 4°C for 24 h, then transferred to 30% sucrose solution until the tissue sank. Coronal hippocampal sections, 20 μm thick, were prepared using a cryostat microtome (Leica, Germany). After returning to room temperature, sections were rinsed with PBS and stained with 0.1% toluidine blue (Solarbio, China) for 10 min at room temperature.

Sections were then rinsed with distilled water, dehydrated through a graded ethanol series, cleared in xylene, and mounted with neutral resin. Images of the hippocampal CA1 region were acquired using an Olympus BX53 microscope (Olympus, Tokyo, Japan). For each animal, three consecutive fields of view were randomly selected at ×400 magnification for analysis. ImageJ software (National Institutes of Health, Bethesda, MD, USA) was used to quantify neuronal density and Nissl-positive area in the CA1 region. Histological injury scores were assessed based on neuronal arrangement, soma morphology, and the integrity of Nissl bodies. All image acquisition and quantitative analyses were performed by investigators blinded to group allocation.

For Western blotting and real-time quantitative PCR (RT-qPCR), bilateral hippocampal tissues were rapidly dissected after anesthesia, snap-frozen in liquid nitrogen, and stored at − 80°C until use.

2.5 Western Blot Analysis

Hippocampal tissues were homogenized on ice in RIPA lysis buffer (Beyotime, Shanghai, China) supplemented with protease and phosphatase inhibitors. Homogenates were centrifuged at 12,000 × g

for 15 min at 4°C, and the supernatants were collected as total protein extracts. Protein concentrations were determined using a BCA protein assay kit (Thermo Fisher Scientific, Waltham, MA, USA). After normalization of protein concentrations, samples were mixed with 5× SDS loading buffer and denatured at 95°C for 5 min.

Equal amounts of total protein, 20–30 μg per lane, were separated by 10% or 12% SDS-PAGE and transferred onto PVDF membranes (Millipore, Billerica, MA, USA). Membranes were blocked with 5% non-fat milk or 5% BSA for phosphorylated proteins at room temperature for 1 h, and then incubated overnight at 4°C with the corresponding primary antibodies listed in Supplementary Table 1. After washing with TBST, membranes were incubated with HRP-conjugated goat anti-rabbit or goat anti-mouse secondary antibodies (Proteintech, Wuhan, China; 1:5000) at room temperature for 1 h.

Protein bands were visualized using enhanced chemiluminescence reagent (ECL; Thermo Fisher Scientific) and imaged with a ChemiDoc™ MP imaging system (Bio-Rad, Hercules, CA, USA). Densitometric analysis was performed using ImageJ software (National Institutes of Health, Bethesda, MD, USA). Except for phosphorylated proteins, protein expression levels were normalized to β-actin. CREB activation was expressed as the p-CREB/CREB ratio.

For detection of linkage-specific ubiquitin signals, antibodies recognizing K63-linked ubiquitin chains and Met1-linked/linear ubiquitin chains were used to assess overall K63-linked and linear ubiquitination patterns in hippocampal tissue. Because these linkage-specific ubiquitin signals are typically detected as high-molecular-weight (HMW) immunoreactive smears, integrated densitometric analysis was performed within a predefined HMW region above the 100-kDa marker, with local background subtraction. The same region-of-interest strategy was applied consistently across groups, and values were normalized to ?-actin. These measurements were used to evaluate overall linkage-specific ubiquitin accumulation in hippocampal lysates rather than ubiquitination of a specific substrate. All Western blot experiments were independently repeated at least three times, and densitometric analyses were performed by investigators blinded to group allocation.

2.6 Quantitative Real-Time PCR

Total RNA was extracted from hippocampal tissue using TRIzol reagent (Invitrogen, Carlsbad, CA, USA). RNA concentration and purity were assessed with a NanoDrop 2000 spectrophotometer (Thermo Fisher Scientific, Wilmington, DE, USA). For each sample, 1 μg of total RNA was reverse-transcribed into cDNA using the PrimeScript™ RT Reagent Kit (Takara Bio Inc., Shiga, Japan) according to the manufacturer's instructions.

Quantitative real-time PCR was performed using TB Green® Premix Ex Taq™ II (Takara Bio Inc.) on an ABI QuantStudio™ 5 Real-Time PCR System (Applied Biosystems, Foster City, CA, USA). Each 20 μL reaction contained 10 μL TB Green Premix, 0.4 μL forward primer (10 μM), 0.4 μL reverse primer (10 μM), 2 μL cDNA template, and 7.2 μL RNase-free water. The cycling conditions were as follows: initial denaturation at 95°C for 30 s, followed by 40 cycles of denaturation at 95°C for 5 s and annealing/extension at 60°C

for 30 s. A melting curve analysis was performed at the end of amplification to confirm product specificity.

Gapdh was used as the internal reference gene, and relative gene expression was calculated using the $2^{-\Delta\Delta Ct}$ method. All samples were analyzed in triplicate, and each experiment was independently repeated at least three times. Primer sequences are listed in Supplementary Table 2.

2.7 Statistical Analysis

Statistical analyses were performed using GraphPad Prism 9.0 (GraphPad Software, San Diego, CA, USA). Data are presented as mean ± SEM. Maternal serum TT_4 and TSH measurements were analyzed at the dam level (n = 15 dams per group). For offspring behavioral, histological, and molecular endpoints, the litter was treated as the unit of biological independence; one male offspring was sampled from each of nine independent litters per group for each endpoint, so n = 9 denotes 9 litters and 9 male offspring, with no multiple pups from the same litter counted as independent observations. Animals were randomly assigned to groups, and behavioral, histological, and molecular analyses were performed by investigators blinded to group allocation. Normality and homogeneity of variance were assessed using the Shapiro-Wilk and Levene's tests, respectively. Two-group comparisons were analyzed using an unpaired two-tailed Student's t-test, whereas comparisons among three groups were analyzed using one-way ANOVA followed by Tukey's multiple-comparisons test. Escape latency in the Morris Water Maze was analyzed using two-way repeated-measures ANOVA followed by Bonferroni post hoc correction. Correlations were assessed using Pearson correlation analysis. No data were excluded except for predefined technical failures. All tests were two-sided, and $P < 0.05$ was considered statistically significant.

3. RESULTS

Maternal thyroid hormone status was assessed to verify successful establishment of the MTHD model. Compared with control dams, MTHD dams showed significantly reduced serum TT_4 levels and significantly elevated serum TSH levels on embryonic day 7, embryonic day 13, and postnatal day 1. This endocrine profile confirmed sustained maternal thyroid hormone deficiency during gestation and the early postnatal period, supporting the validity of the model used for subsequent offspring analyses (Supplementary Table 3).

3.1 Maternal Thyroid Hormone Deficiency Induces Autism-Related and Cognitive Behavioral Abnormalities

To determine the long-term impact of MTHD on offspring neurodevelopment, we performed a multidimensional behavioral assessment in adolescent male offspring (Fig. 1a).

In the three-chamber social test, offspring in the Control group showed a consistent preference for the unfamiliar rat and preserved social novelty recognition. In contrast, MTHD offspring spent significantly

less time interacting with the stranger rat, showed a marked reduction in the social preference index, and exhibited further decreases in exploration of the novel stranger rat (all $P < 0.01$), indicating impairments in both social interaction and social novelty recognition (Fig. 1b).

In the open field test, MTHD offspring showed significantly reduced time spent in the center zone and fewer center entries ($P < 0.01$), whereas total distance traveled was not significantly changed ($P > 0.05$). These findings suggest that spontaneous locomotor activity was largely preserved, while exploratory behavior was reduced and anxiety-like behavior was increased (Fig. 1c).

Assessment of repetitive stereotyped behavior further showed that self-grooming duration was significantly increased in the MTHD group ($P < 0.01$) (Fig. 1d). During Morris Water Maze acquisition training, escape latency remained consistently longer in MTHD offspring than in Controls, with an overall rightward shift of the learning curve and increased path length (Fig. 1f,g). In the probe trial, MTHD offspring showed altered swim paths, reduced time in the target quadrant, fewer platform crossings, and increased latency to cross the former platform location, indicating impaired hippocampus-dependent spatial learning and memory retention (Fig. 1e,h,i).

Together, these data show that MTHD produced an adolescent phenotype characterized by impaired social interaction and novelty recognition, increased repetitive grooming, anxiety-like behavior, and deficits in hippocampus-dependent learning and memory. The social and repetitive behavioral changes are relevant to core behavioral domains studied in experimental autism research, whereas the anxiety-like and cognitive findings indicate broader neurodevelopmental effects.

Figure 1. Maternal thyroid hormone deficiency induces neurodevelopmental behavioral abnormalities in offspring. (a) Experimental workflow showing maternal thyroid hormone deficiency (MTHD) or control exposure from gestational day 0 (GD0) to GD21, weaning at PND21, behavioral testing during PND35-PND50, and hippocampal tissue collection at PND50. (b) Representative movement traces and quantification from the three-chamber social test showing reduced social preference in MTHD offspring. (c) Representative open-field movement traces and quantification of total distance, time in the center zone, and center entries. (d) Representative self-grooming behavior and quantification of grooming time. (e) Representative Morris water maze probe-trial swim paths and quantification of time in the target quadrant and escape-passage latency. (f) Escape latency during Morris water maze acquisition training. (g) Path length during Morris water maze acquisition training. (h) Probe-trial mean swim speed and time in the former platform quadrant. (i) Probe-trial platform crossings within 60 s and latency to cross the former platform location. Data are presented as mean ± SEM, n = 9 biologically independent male offspring from 9 independent litters per group. Between-group comparisons were performed using an unpaired two-tailed Student's t-test; acquisition training in the Morris water maze was analyzed using two-way repeated-measures ANOVA followed by Bonferroni post hoc correction. ns, not significant; *$P < 0.05$, **$P < 0.01$.

3.2 Maternal Thyroid Hormone Deficiency Disrupts Hippocampal Neuronal Architecture

To determine the effects of maternal thyroid hormone deficiency on the hippocampus of offspring, we first examined the overall hippocampal anatomy, with particular focus on the CA1 region, which is closely involved in learning and memory (Fig. 2a). Within the canonical hippocampal trisynaptic circuit, CA1 serves as the final integrative node of the DG-CA3-CA1 pathway and represents a major hippocampal output region essential for spatial learning and memory formation (Fig. 2c). Therefore, CA1 was selected as the primary region for subsequent histological analysis.

Nissl staining showed that, compared with the Control group, the CA1 region in MTHD offspring exhibited marked neuronal disorganization, reduced neuronal density, shrunken cell bodies, weaker Nissl staining, and partial vacuolar degeneration, together with impaired structural integrity (Fig. 2b). Quantitative analysis further showed that the Nissl-positive area in CA1 was significantly reduced in the MTHD group ($P < 0.01$; Fig. 2d), whereas the neuronal injury score was markedly increased ($P < 0.01$; Fig. 2e). Neuronal morphological integrity was also significantly decreased ($P < 0.01$; Fig. 2f).

Thus, MTHD was associated with reduced neuronal integrity in the hippocampal CA1 region, providing a structural correlate for the observed changes in synaptic protein expression and hippocampus-dependent behavior.

Figure 2. Maternal thyroid hormone deficiency impairs neuronal cytoarchitecture in the hippocampal CA1 region of offspring. (a) Schematic coronal anatomy of the adult rat hippocampus showing the major hippocampal subregions, including CA1, CA3 and the dentate gyrus (DG). (b) Representative Nissl-stained images of the hippocampal CA1 region in Control and MTHD offspring. (c) Schematic of the hippocampal CA1 neural circuit, illustrating inputs from CA3 Schaffer collaterals and perforant-path projections from the entorhinal cortex, and output projections to the subiculum. (d) Quantification of the Nissl-positive area in the CA1 region. (e) Quantification of the tissue injury score in the CA1 region. (f) Quantification of neuronal morphological integrity in the CA1 region. Data are presented as mean ± SEM, n = 9 biologically independent male offspring from 9 independent litters per group. Between-group comparisons were performed using an unpaired two-tailed Student's t-test. $^{**}P < 0.01$.

3.3 Maternal Thyroid Hormone Deficiency Suppresses CYLD Expression and Disrupts Hippocampal Deubiquitination Homeostasis

To investigate the molecular mechanisms underlying MTHD-induced hippocampal injury, we examined the key deubiquitinase CYLD and markers related to ubiquitin homeostasis (Fig. 3). Western blot analysis showed that hippocampal CYLD protein expression was significantly reduced in the MTHD group compared with the Control group ($P < 0.01$). RT-qPCR further confirmed a parallel decrease in Cyld mRNA expression ($P < 0.01$), indicating that MTHD suppresses CYLD expression at the transcriptional level (Fig. 3a-c).

Because CYLD regulates non-degradative ubiquitin linkages, we next assessed linkage-specific ubiquitin signals in hippocampal lysates. HMW K63-linked ubiquitin signals were markedly increased in the MTHD

group ($P < 0.01$), and HMW linear/Met1-linked ubiquitin signals were also significantly increased ($P < 0.01$), suggesting an alteration in hippocampal linkage-specific ubiquitin homeostasis (Fig. 3d,e).

Thus, CYLD downregulation and increased non-degradative ubiquitin signals were concurrent molecular features of the offspring hippocampus after MTHD exposure.

Figure 3. Maternal thyroid hormone deficiency disrupts CYLD-associated ubiquitin homeostasis in the hippocampus. (a) Representative Western blots showing hippocampal CYLD protein expression in Control and MTHD offspring. (b) Quantification of hippocampal CYLD protein expression. (c) RT-qPCR analysis of Cyld mRNA expression. (d) Western blot analysis and quantification of K63-linked ubiquitin signals in the high-molecular-weight region. (e) Western blot analysis and quantification of linear/Met1-linked ubiquitin signals in the high-molecular-weight region. Data are presented as mean ± SEM, n = 9 biologically independent male offspring from 9 independent litters per group. Between-group comparisons were performed using an unpaired two-tailed Student's t-test. $^{**}P < 0.01$.

3.4 Maternal Thyroid Hormone Deficiency Reduces Hippocampal Synapse-Related Protein Expression

Given the critical role of synaptic protein homeostasis in neuronal communication and synaptic plasticity, we next examined changes in hippocampal synapse-related proteins (Fig. 4).

Western blot analysis showed that PSD95 protein levels were significantly lower in the MTHD group than in the Control group ($P < 0.01$) (Fig. 4a,b). In parallel, the expression levels of Synaptophysin and Synapsin I were also markedly reduced ($P < 0.001$ and $P < 0.01$, respectively) (Fig. 4a,c,d). Further analysis revealed a significant decrease in the excitatory synaptic AMPA receptor subunit GluA1 in the MTHD group ($P < 0.01$) (Fig. 4a,e).

Thus, MTHD reduced proteins representing postsynaptic scaffolding, presynaptic vesicle regulation, and excitatory AMPA receptor signaling in the offspring hippocampus.

Figure 4. Maternal thyroid hormone deficiency disrupts hippocampal synaptic protein homeostasis. (a) Representative Western blots showing hippocampal expression of the synapse-associated proteins PSD95, synaptophysin, Synapsin I and GluA1. (b) Quantification of PSD95 protein expression. (c) Quantification of synaptophysin protein expression. (d) Quantification of Synapsin I protein expression. (e) Quantification of GluA1 protein expression. Data are presented as mean ± SEM, n = 9 biologically independent male offspring from 9 independent litters per group. Between-group comparisons were performed using an unpaired two-tailed Student’s t-test. $^{**}P < 0.01$, $^{***}P < 0.001$.

3.5 Abnormal Synaptic Protein Homeostasis Is Accompanied by Sustained Suppression of Neurotrophic Signaling

Because the BDNF-CREB signaling axis plays an essential role in neuronal development, synaptic plasticity, and learning and memory, we further examined the expression of hippocampal BDNF and CREB-related signaling molecules (Fig. 5). Western blot analysis showed that hippocampal BDNF protein expression was significantly reduced in the MTHD group compared with the Control group ($P < 0.001$) (Fig. 5a,b). In addition, p-CREB (Ser133) levels were markedly decreased ($P < 0.01$) (Fig. 5a,c), and total CREB expression was also significantly reduced ($P < 0.001$) (Fig. 5a,d). RT-qPCR analysis further showed that hippocampal Bdnf mRNA expression was significantly lower in the MTHD group than in Controls ($P < 0.01$) (Fig. 5e), consistent with the changes observed at the protein level.

Correlation analysis showed that BDNF protein expression was positively correlated with CYLD protein expression ($r = 0.72$, $P < 0.01$) and with PSD95 protein expression ($r = 0.66$, $P < 0.01$) (Fig. 5f).

Thus, MTHD reduced hippocampal BDNF-CREB signaling, and BDNF abundance covaried positively with CYLD and PSD95 expression.

Figure 5. Maternal thyroid hormone deficiency suppresses hippocampal BDNF-CREB neurotrophic signaling. (a) Representative Western blots showing hippocampal expression of BDNF, phosphorylated CREB at Ser133 [p-CREB (Ser133)] and total CREB. (b) Quantification of BDNF protein expression. (c) Quantification of p-CREB (Ser133) protein expression. (d) Quantification of total CREB protein expression. (e) RT-qPCR analysis of Bdnf mRNA expression. (f) Pearson correlation analyses showing the relationships between BDNF protein expression and CYLD protein expression, and between BDNF protein expression and PSD95 protein expression. Data are presented as mean ± SEM, n = 9 biologically independent male offspring from 9 independent litters per group. Between-group comparisons were performed using an unpaired two-tailed Student's t-test; correlations were assessed using Pearson correlation analysis. $^{**}P < 0.01$, $^{***}P < 0.001$.

3.6 Postnatal CYLD Overexpression Improves Ubiquitin Homeostasis, Synaptic Protein Expression, and Behavior

To further determine the role of CYLD in neurodevelopmental abnormalities induced by maternal thyroid hormone deficiency (MTHD), AAV-mediated bilateral hippocampal CYLD overexpression (AAV-CYLD) was performed in offspring on postnatal day 28 (P28). After approximately 3–4 weeks of viral expression, behavioral testing was conducted at P50-P60, followed by hippocampal tissue collection for molecular analyses (Fig. 6a).

We first evaluated the efficacy of viral intervention by measuring hippocampal CYLD protein expression. Western blot analysis showed that CYLD expression was significantly reduced in the MTHD + AAV-GFP group compared with the Control + AAV-GFP group ($P < 0.001$). After AAV-CYLD treatment, hippocampal CYLD protein levels were markedly restored and were significantly higher than those in the MTHD + AAV-GFP group ($P < 0.001$), reaching levels close to those observed in Controls (Fig. 6b). These results indicate that AAV-CYLD effectively restores hippocampal CYLD expression in MTHD offspring.

We next assessed K63-linked ubiquitination. MTHD markedly increased total hippocampal K63-linked ubiquitination (P < 0.001), whereas AAV-CYLD treatment significantly reduced K63-linked ubiquitination levels (P < 0.01) (Fig. 6c). This finding supports the interpretation that CYLD overexpression attenuates MTHD-associated disruption of linkage-specific ubiquitin homeostasis.

Further analysis of synapse-related proteins showed that PSD95, Synapsin I, and GluA1 expression levels were all significantly lower in the MTHD group than in Controls (all $P < 0.001$). After AAV-CYLD intervention, the expression of these synaptic proteins was significantly increased compared with the MTHD + AAV-GFP group (all $P < 0.01$) (Fig. 6d), suggesting that CYLD overexpression partially restores synaptic protein homeostasis under MTHD conditions.

In the Three-Chamber Social Test, AAV-CYLD significantly improved MTHD-induced social deficits. Compared with the MTHD + AAV-GFP group, MTHD offspring receiving AAV-CYLD spent more time interacting with the stranger rat and showed a higher social preference index, indicating restored social interaction and social preference (Fig. 6e).

In the Open Field Test, AAV-CYLD also alleviated MTHD-induced anxiety-like behavior. MTHD + AAV-CYLD offspring showed increased center-zone residence time, more center-zone entries, and enhanced rearing behavior compared with the MTHD + AAV-GFP group, whereas total distance traveled was not significantly altered, indicating improved exploratory behavior without a nonspecific change in locomotor activity (Fig. 6f).

Finally, spatial learning and memory were assessed using the Morris Water Maze. During acquisition training, the MTHD + AAV-GFP group showed prolonged escape latency, whereas AAV-CYLD treatment progressively shortened escape latency from training day 2 onward, with a clear improvement during the later training phase (Fig. 6g). In the probe trial, MTHD offspring showed reduced time spent in the target quadrant and fewer platform crossings, while AAV-CYLD treatment significantly increased both measures (both $P < 0.01$) (Fig. 6h). These results show that postnatal CYLD overexpression improves MTHD-induced deficits in hippocampus-dependent spatial learning and memory.

Together, these rescue experiments show that postnatal hippocampal CYLD overexpression counteracted MTHD-associated CYLD loss, reduced K63-linked ubiquitin accumulation, partially restored PSD95, Synapsin I, and GluA1 expression, and improved social, anxiety-like, and hippocampus-dependent cognitive outcomes. These findings provide functional evidence that CYLD-associated ubiquitin homeostasis contributes to a subset of the molecular and behavioral abnormalities induced by MTHD.

Figure 6. Postnatal hippocampal CYLD overexpression attenuates K63-linked ubiquitin accumulation and improves synaptic and behavioral outcomes in MTHD offspring. (a) Schematic of the AAV-mediated hippocampal CYLD overexpression experiment. Male offspring received bilateral stereotaxic hippocampal injections of AAV-GFP or AAV-CYLD at postnatal day 28 (P28), followed by behavioral testing at P50-P60 and hippocampal tissue collection for molecular analyses. (b) Representative Western blots and quantification of hippocampal CYLD protein expression. (c) Representative Western

blots and quantification of K63-linked ubiquitin signals in the high-molecular-weight region. (d) Representative Western blots and quantification of synapse-associated proteins, including PSD95, Synapsin I, and GluA1. (e) Quantification of social interaction time and social preference index in the three-chamber social test. (f) Quantification of center-zone residence time, center entries, rearing behavior, and total locomotor distance in the open field test. (g) Morris water maze analysis, including escape latency during acquisition training, representative probe-trial swim paths, and latency to cross the former platform location. Data are presented as mean ± SEM. Sample sizes are indicated by individual data points in each graph; each point represents one biologically independent male offspring from an independent litter. For Western blot analyses, representative blots are shown, and densitometric quantification was performed using independent biological samples. Escape latency during acquisition training was analyzed using two-way repeated-measures ANOVA followed by Bonferroni post hoc correction; other comparisons were analyzed using one-way ANOVA followed by Tukey's multiple-comparisons test. ns, not significant; *$P < 0.05$, **$P < 0.01$, ***$P < 0.001$.

4. DISCUSSION

The principal finding of this study is that CYLD-associated K63-linked ubiquitin dysregulation contributes to persistent synaptic and behavioral abnormalities after MTHD. Ubiquitin chains regulate both proteasome-independent signaling and the organization of protein complexes [19, 20]. In MTHD offspring, reduced hippocampal CYLD expression coincided with increased K63-linked ubiquitin signals, lower synaptic protein abundance, and autism-related behavioral abnormalities. Postnatal CYLD restoration partially reversed these molecular and behavioral changes. These data identify altered ubiquitin homeostasis as a functional molecular layer connecting gestational endocrine disruption to postnatal neurodevelopmental phenotypes.

CYLD is a plausible regulatory node because it preferentially cleaves K63-linked and linear ubiquitin chains [21, 22]. These non-degradative chains organize signaling complexes, trafficking events, and spatially restricted protein interactions [23, 24]. Reduced CYLD expression and increased K63-linked ubiquitin signals are therefore consistent with impaired control of synaptic protein organization or trafficking. However, the present immunoblot analyses measured global linkage-specific signals in whole hippocampal lysates. They do not identify direct CYLD substrates, modified lysine residues, or the relevant cell types. Ubiquitin-remnant proteomics and site-resolved approaches will be required to establish those substrate-level mechanisms [25, 26].

The AAV-CYLD experiment extends the association by testing whether postnatal restoration of CYLD modifies the MTHD phenotype. Viral approaches provide spatially targeted tools for manipulating neural pathways and testing functional contributions in vivo [27, 28]. CYLD restoration reduced K63-linked ubiquitin accumulation and increased PSD95, Synapsin I, and GluA1 expression. It also improved social interaction, center-zone exploration, and spatial learning and memory. These effects are consistent with established roles of CYLD and other deubiquitinases in cellular signaling and nervous-system homeostasis [29, 30]. Nevertheless, rescue after overexpression does not establish that endogenous

CYLD loss is necessary or sufficient for the phenotype, nor does it exclude effects mediated through broader protein-turnover pathways [31].

The coordinated changes in PSD95, Synapsin I, and GluA1 suggest disruption across multiple components of the excitatory synapse. PSD95 organizes postsynaptic signaling complexes [32, 33], Synapsin I regulates presynaptic vesicle availability [34], and GluA1 contributes to AMPA receptor trafficking and excitatory transmission [35, 36]. Their concurrent reduction is compatible with impaired coordination between presynaptic release, postsynaptic scaffolding, and receptor availability [37]. Ubiquitin-dependent regulation can influence neuronal protein turnover, receptor trafficking, and postsynaptic plasticity [38, 39]. The partial restoration of all three proteins after CYLD overexpression therefore supports a pathway-level relationship between K63-linked ubiquitin homeostasis and synaptic protein organization. Electrophysiology and ultrastructural analyses are needed to determine whether these molecular changes translate into altered synaptic transmission or plasticity.

Reduced BDNF-CREB signaling provides a second molecular feature relevant to activity-dependent synaptic maturation. BDNF-TrkB signaling regulates neural-circuit development, long-term potentiation, and learning [40, 41], whereas CREB-dependent transcription supports activity-regulated synaptic plasticity [42, 43]. MTHD reduced BDNF, Bdnf mRNA, p-CREB, and total CREB, and BDNF abundance correlated positively with CYLD and PSD95. These correlations place neurotrophic signaling, CYLD loss, and synaptic protein disruption within the same molecular state. They do not establish directionality. Future experiments should test whether BDNF-CREB signaling lies downstream of CYLD-dependent ubiquitin regulation or changes in parallel after MTHD.

The postnatal rescue also indicates that the consequences of prenatal MTHD retain a degree of developmental plasticity. Cross-species comparisons show that postnatal rodent brain maturation overlaps with several prenatal and early postnatal stages of human neural development [44]. Early-life exposures can program long-term neurodevelopmental outcomes, but their effects vary across developmental windows [45, 46]. CYLD overexpression at postnatal day 28 therefore demonstrates experimental modifiability within this rat model, not a directly translatable therapeutic window. The intervention was localized to the hippocampus, whereas the measured social, repetitive, and anxiety-related behaviors depend on distributed neural circuits.

The relevance to autism is supported by convergence at the levels of behavior and synaptic biology, but it requires careful interpretation. Synaptic dysfunction and altered plasticity are recurrent features of autism-associated genetic conditions [47, 48]. Experimental studies further implicate excitation-inhibition balance, social-reward circuitry, and corticostriatal maturation in social and repetitive behavioral phenotypes [49–52]. MTHD offspring showed reduced social interaction and novelty recognition together with increased repetitive grooming, which model behavioral domains relevant to autism research. Anxiety-like behavior and spatial learning deficits are not autism-specific. Accordingly, this study should be interpreted as identifying an autism-relevant molecular and behavioral pathway after a prenatal endocrine exposure, rather than establishing MTHD offspring as a complete model of autism.

Several limitations define the scope of this interpretation. Only male offspring were studied, and the sample size was modest. Analyses were restricted mainly to whole hippocampal tissue, preventing resolution of cell-type-specific ubiquitin changes and limiting inference about distributed social and repetitive-behavior circuits. The rescue experiment tested sufficiency of increased CYLD activity but not the necessity, timing, or endogenous substrates of CYLD loss. Despite these limitations, the combined exposure, molecular, synaptic, and rescue data support CYLD-associated K63-linked ubiquitin homeostasis as a modifiable contributor to MTHD-induced neurodevelopmental abnormalities. This framework links a gestational endocrine risk factor to a post-translational pathway relevant to synaptic dysfunction and autism-related behavior.

5. CONCLUSION

This study identifies sustained disruption of CYLD-associated K63-linked ubiquitin homeostasis as a functionally relevant molecular pathway in the offspring hippocampus after MTHD. MTHD reduced CYLD expression, increased non-degradative ubiquitin signals, disrupted synaptic protein networks, attenuated BDNF-CREB signaling, and produced social, repetitive, anxiety-like, and cognitive abnormalities. Postnatal hippocampal CYLD overexpression reduced K63-linked ubiquitin accumulation, partially restored synapse-associated protein expression, and improved social, anxiety-like, and hippocampus-dependent cognitive outcomes. Together, these findings connect gestational endocrine disruption to altered ubiquitin signaling, impaired synaptic maturation, and autism-related behavioral phenotypes. Identification of direct CYLD substrates and validation across sex, cell type, brain region, and developmental stage will be required to define the broader relevance of this pathway to autism pathobiology.

Declarations

Ethics approval

All experimental procedures were approved by the Ethics Committee for the Use and Care of Laboratory Animals of China Medical University.

Competing interests

The authors declare that they have no competing interests.

Funding

This study was supported by the National Natural Science Foundation of China (Grant No. 81200573).

Author contributions

Dijie Liu conceived and designed the study, supervised the project, interpreted the data, and drafted and revised the manuscript. Kai Tao contributed to experimental coordination, data interpretation, and manuscript revision. Shiyong Wang contributed to behavioral testing, histological analysis, and figure preparation. Shu Liu performed molecular experiments and contributed to data analysis. Ying Sun contributed to the establishment of the animal model, AAV intervention, behavioral experiments, and data acquisition. All authors reviewed and approved the final manuscript.

Acknowledgements

Not applicable.

Availability of data and materials

The data sets used and/or analyzed during the current study are available from the corresponding author on reasonable request.

References

1. Mohan, V., Sinha, R.A., Pathak, A., Rastogi, L., Kumar, P., Pal, A., et al.: Maternal thyroid hormone deficiency affects the fetal neocorticogenesis by reducing the proliferating pool, rate of neurogenesis and indirect neurogenesis. Exp. Neurol. **237**, 477–488 (2012). https://doi.org/10.1016/j.expneurol.2012.07.019
2. Bernal, J.: Thyroid hormone receptors in brain development and function. Nat. Clin. Pract. Endocrinol. Metab. **3**, 249–259 (2007). https://doi.org/10.1038/ncpendmet0424
3. Thompson, W., Russell, G., Baragwanath, G., Matthews, J., Vaidya, B., Thompson-Coon, J.: Maternal thyroid hormone insufficiency during pregnancy and risk of neurodevelopmental disorders in offspring: a systematic review and meta-analysis. Clin. Endocrinol. (Oxf). **88**, 575–584 (2018). https://doi.org/10.1111/cen.13550
4. Alvarez-Castelao, B., Schuman, E.M.: The Regulation of Synaptic Protein Turnover. J. Biol. Chem. **290**, 28623–28630 (2015). https://doi.org/10.1074/jbc.R115.657130
5. Dörrbaum, A.R., Kochen, L., Langer, J.D., Schuman, E.M.: Local and global influences on protein turnover in neurons and glia. eLife. **7**, e34202 (2018). https://doi.org/10.7554/eLife.34202
6. Cizeron, M., Qiu, Z., Koniaris, B., Gokhale, R., Komiyama, N.H., Fransén, E., et al.: A brainwide atlas of synapses across the mouse life span. Science. **369**, 270–275 (2020). https://doi.org/10.1126/science.aba3163
7. Forrest, M.P., Parnell, E., Penzes, P.: Dendritic structural plasticity and neuropsychiatric disease. Nat. Rev. Neurosci. **19**, 215–234 (2018). https://doi.org/10.1038/nrn.2018.16

8. Swatek, K.N., Komander, D.: Ubiquitin modifications. Cell. Res. **26**, 399–422 (2016). https://doi.org/10.1038/cr.2016.39
9. Erpapazoglou, Z., Walker, O., Haguenauer-Tsapis, R.: Versatile Roles of K63-Linked Ubiquitin Chains in Trafficking. Cells. **3**, 1027–1088 (2014). https://doi.org/10.3390/cells3041027
10. Yau, R., Rape, M.: The increasing complexity of the ubiquitin code. Nat. Cell. Biol. **18**, 579–586 (2016). https://doi.org/10.1038/ncb3358
11. Komander, D., Rape, M.: The Ubiquitin Code. Annu. Rev. Biochem. **81**, 203–229 (2012). https://doi.org/10.1146/annurev-biochem-060310-170328
12. Brummelkamp, T.R., Nijman, S.M.B., Dirac, A.M.G., Bernards, R.: Loss of the cylindromatosis tumour suppressor inhibits apoptosis by activating NF-κB. Nature. **424**, 797–801 (2003). https://doi.org/10.1038/nature01811
13. Kovalenko, A., Chable-Bessia, C., Cantarella, G., Israël, A., Wallach, D., Courtois, G.: The tumour suppressor CYLD negatively regulates NF-κB signalling by deubiquitination. Nature. **424**, 801–805 (2003). https://doi.org/10.1038/nature01802
14. Liu, D., Tao, K., Sun, Y., Hao, J., Wang, S.: The role of the Wnt/BDNF pathway in maternal SCH-induced autism-like phenotypes in offspring rats: behavioral and molecular mechanisms. Transl Psychiatry. **15**, 387 (2025). https://doi.org/10.1038/s41398-025-03570-6
15. Moy, S.S., Nadler, J.J., Perez, A., Barbaro, R.P., Johns, J.M., Magnuson, T.R., et al.: Sociability and preference for social novelty in five inbred strains: an approach to assess autistic-like behavior in mice. Genes Brain Behav. **3**, 287–302 (2004). https://doi.org/10.1111/j.1601-1848.2004.00076.x
16. Seibenhener, M.L., Wooten, M.C.: Use of the Open Field Maze to Measure Locomotor and Anxiety-like Behavior in Mice. JoVE. 52434 (2015). https://doi.org/10.3791/52434
17. Kalueff, A.V., Stewart, A.M., Song, C., Berridge, K.C., Graybiel, A.M., Fentress, J.C.: Neurobiology of rodent self-grooming and its value for translational neuroscience. Nat. Rev. Neurosci. **17**, 45–59 (2016). https://doi.org/10.1038/nrn.2015.8
18. Vorhees, C.V., Williams, M.T.: Morris water maze: procedures for assessing spatial and related forms of learning and memory. Nat. Protoc. **1**, 848–858 (2006). https://doi.org/10.1038/nprot.2006.116
19. Hicke, L., Schubert, H.L., Hill, C.P.: Ubiquitin-binding domains. Nat. Rev. Mol. Cell. Biol. **6**, 610–621 (2005). https://doi.org/10.1038/nrm1701
20. Mukhopadhyay, D., Riezman, H.: Proteasome-independent functions of ubiquitin in endocytosis and signaling. Science. **315**, 201–205 (2007). https://doi.org/10.1126/science.1127085
21. Sato, Y., Yoshikawa, A., Yamagata, A., Mimura, H., Yamashita, M., Ookata, K., et al.: Structural basis for specific cleavage of Lys 63-linked polyubiquitin chains. Nature. **455**, 358–362 (2008). https://doi.org/10.1038/nature07254
22. Komander, D., Reyes-Turcu, F., Licchesi, J.D.F., Odenwaelder, P., Wilkinson, K.D., Barford, D.: Molecular discrimination of structurally equivalent Lys 63-linked and linear polyubiquitin chains. EMBO Rep. **10**, 466–473 (2009). https://doi.org/10.1038/embor.2009.55

23. Grabbe, C., Husnjak, K., Dikic, I.: The spatial and temporal organization of ubiquitin networks. Nat. Rev. Mol. Cell. Biol. **12**, 295–307 (2011). https://doi.org/10.1038/nrm3099
24. Husnjak, K., Dikic, I.: Ubiquitin-binding proteins: decoders of ubiquitin-mediated cellular functions. Annu. Rev. Biochem. **81**, 291–322 (2012). https://doi.org/10.1146/annurev-biochem-051810-094654
25. Akimov, V., Barrio-Hernandez, I., Hansen, S.V.F., Hallenborg, P., Pedersen, A.-K., Bekker-Jensen, D.B., et al.: UbiSite approach for comprehensive mapping of lysine and N-terminal ubiquitination sites. Nat. Struct. Mol. Biol. **25**, 631–640 (2018). https://doi.org/10.1038/s41594-018-0084-y
26. Udeshi, N.D., Svinkina, T., Mertins, P., Kuhn, E., Mani, D.R., Qiao, J.W., et al.: Refined Preparation and Use of Anti-diglycine Remnant (K-ε-GG) Antibody Enables Routine Quantification of 10,000s of Ubiquitination Sites in Single Proteomics Experiments. Mol. Cell. Proteom. **12**, 825–831 (2013). https://doi.org/10.1074/mcp.O112.027094
27. Luo, L., Callaway, E.M., Svoboda, K.: Genetic Dissection of Neural Circuits: A Decade of Progress. Neuron. **98**, 865 (2018). https://doi.org/10.1016/j.neuron.2018.05.004
28. Madisen, L., Zwingman, T.A., Sunkin, S.M., Oh, S.W., Zariwala, H.A., Gu, H., et al.: A robust and high-throughput Cre reporting and characterization system for the whole mouse brain. Nat. Neurosci. **13**, 133–140 (2010). https://doi.org/10.1038/nn.2467
29. Sun, S.C.: CYLD: a tumor suppressor deubiquitinase regulating NF-kappaB activation and diverse biological processes. Cell. Death Differ. **17**, 25–34 (2010). https://doi.org/10.1038/cdd.2009.43
30. Todi, S.V., Paulson, H.L.: Balancing act: deubiquitinating enzymes in the nervous system. Trends Neurosci. **34**, 370–382 (2011). https://doi.org/10.1016/j.tins.2011.05.004
31. Bingol, B., Sheng, M.: Deconstruction for reconstruction: the role of proteolysis in neural plasticity and disease. Neuron. **69**, 22–32 (2011). https://doi.org/10.1016/j.neuron.2010.11.006
32. Kim, E., Sheng, M.: PDZ domain proteins of synapses. Nat. Rev. Neurosci. **5**, 771–781 (2004). https://doi.org/10.1038/nrn1517
33. Sheng, M., Kim, E.: The postsynaptic organization of synapses. Cold Spring Harb Perspect. Biol. **3**, a005678 (2011). https://doi.org/10.1101/cshperspect.a005678
34. Cesca, F., Baldelli, P., Valtorta, F., Benfenati, F.: The synapsins: key actors of synapse function and plasticity. Prog Neurobiol. **91**, 313–348 (2010). https://doi.org/10.1016/j.pneurobio.2010.04.006
35. Henley, J.M., Wilkinson, K.A.: Synaptic AMPA receptor composition in development, plasticity and disease. Nat. Rev. Neurosci. **17**, 337–350 (2016). https://doi.org/10.1038/nrn.2016.37
36. Shepherd, J.D., Huganir, R.L.: The cell biology of synaptic plasticity: AMPA receptor trafficking. Annu. Rev. Cell. Dev. Biol. **23** (2007). https://doi.org/10.1146/annurev.cellbio.23.090506.123516 :613 – 43
37. Biederer, T., Kaeser, P.S., Blanpied, T.A.: Transcellular nanoalignment of synaptic function. Neuron. **96**, 680–696 (2017). https://doi.org/10.1016/j.neuron.2017.10.006
38. Tai, H.C., Schuman, E.M.: Ubiquitin, the proteasome and protein degradation in neuronal function and dysfunction. Nat. Rev. Neurosci. **9**, 826–838 (2008). https://doi.org/10.1038/nrn2499

39. Mabb, A.M., Ehlers, M.D.: Ubiquitination in postsynaptic function and plasticity. Annu. Rev. Cell. Dev. Biol. **26**, 179–210 (2010). https://doi.org/10.1146/annurev-cellbio-100109-104129
40. Park, H., Poo, M.M.: Neurotrophin regulation of neural circuit development and function. Nat. Rev. Neurosci. **14**, 7–23 (2013). https://doi.org/10.1038/nrn3379
41. Minichiello, L.: TrkB signalling pathways in LTP and learning. Nat. Rev. Neurosci. **10**, 850–860 (2009). https://doi.org/10.1038/nrn2738
42. West, A.E., Greenberg, M.E.: Neuronal activity-regulated gene transcription in synapse development and cognitive function. Cold Spring Harb Perspect. Biol. **3**, a005744 (2011). https://doi.org/10.1101/cshperspect.a005744
43. Benito, E., Barco, A.: CREB's control of intrinsic and synaptic plasticity: implications for CREB-dependent memory models. Trends Neurosci. **33**, 230–240 (2010). https://doi.org/10.1016/j.tins.2010.02.001
44. Semple, B.D., Blomgren, K., Gimlin, K., Ferriero, D.M., Noble-Haeusslein, L.J.: Brain development in rodents and humans: identifying benchmarks of maturation and vulnerability to injury across species. Prog Neurobiol. **106–107**, 1–16 (2013). https://doi.org/10.1016/j.pneurobio.2013.04.001
45. Bale, T.L., Baram, T.Z., Brown, A.S., Goldstein, J.M., Insel, T.R., McCarthy, M.M., et al.: Early life programming and neurodevelopmental disorders. Biol. Psychiatry. **68**, 314–319 (2010). https://doi.org/10.1016/j.biopsych.2010.05.028
46. Rice, D., Barone, S. Jr.: Critical periods of vulnerability for the developing nervous system: evidence from humans and animal models. Environ. Health Perspect. **108** (2000). Suppl 3:511 – 33 https://doi.org/10.1289/ehp.00108s3511
47. Bourgeron, T.: From the genetic architecture to synaptic plasticity in autism spectrum disorder. Nat. Rev. Neurosci. **16**, 551–563 (2015). https://doi.org/10.1038/nrn3992
48. Zoghbi, H.Y., Bear, M.F.: Synaptic dysfunction in neurodevelopmental disorders associated with autism and intellectual disabilities. Cold Spring Harb Perspect. Biol. **4**, a009886 (2012). https://doi.org/10.1101/cshperspect.a009886
49. Yizhar, O., Fenno, L.E., Prigge, M., Schneider, F., Davidson, T.J., O'Shea, D.J., et al.: Neocortical excitation/inhibition balance in information processing and social dysfunction. Nature. **477**, 171–178 (2011). https://doi.org/10.1038/nature10360
50. Bariselli, S., Tzanoulinou, S., Glangetas, C., Prévost-Solié, C., Pucci, L., Viguié, J., et al.: SHANK3 controls maturation of social reward circuits in the VTA. Nat. Neurosci. **19**, 926–934 (2016). https://doi.org/10.1038/nn.4319
51. Barak, B., Feng, G.: Neurobiology of social behavior abnormalities in autism and Williams syndrome. Nat. Neurosci. **19**, 647–655 (2016). https://doi.org/10.1038/nn.4276
52. Peixoto, R.T., Wang, W., Croney, D.M., Kozorovitskiy, Y., Sabatini, B.L.: Early hyperactivity and precocious maturation of corticostriatal circuits in Shank3B-/- mice. Nat. Neurosci. **19**, 716–724 (2016). https://doi.org/10.1038/nn.4260

Figures

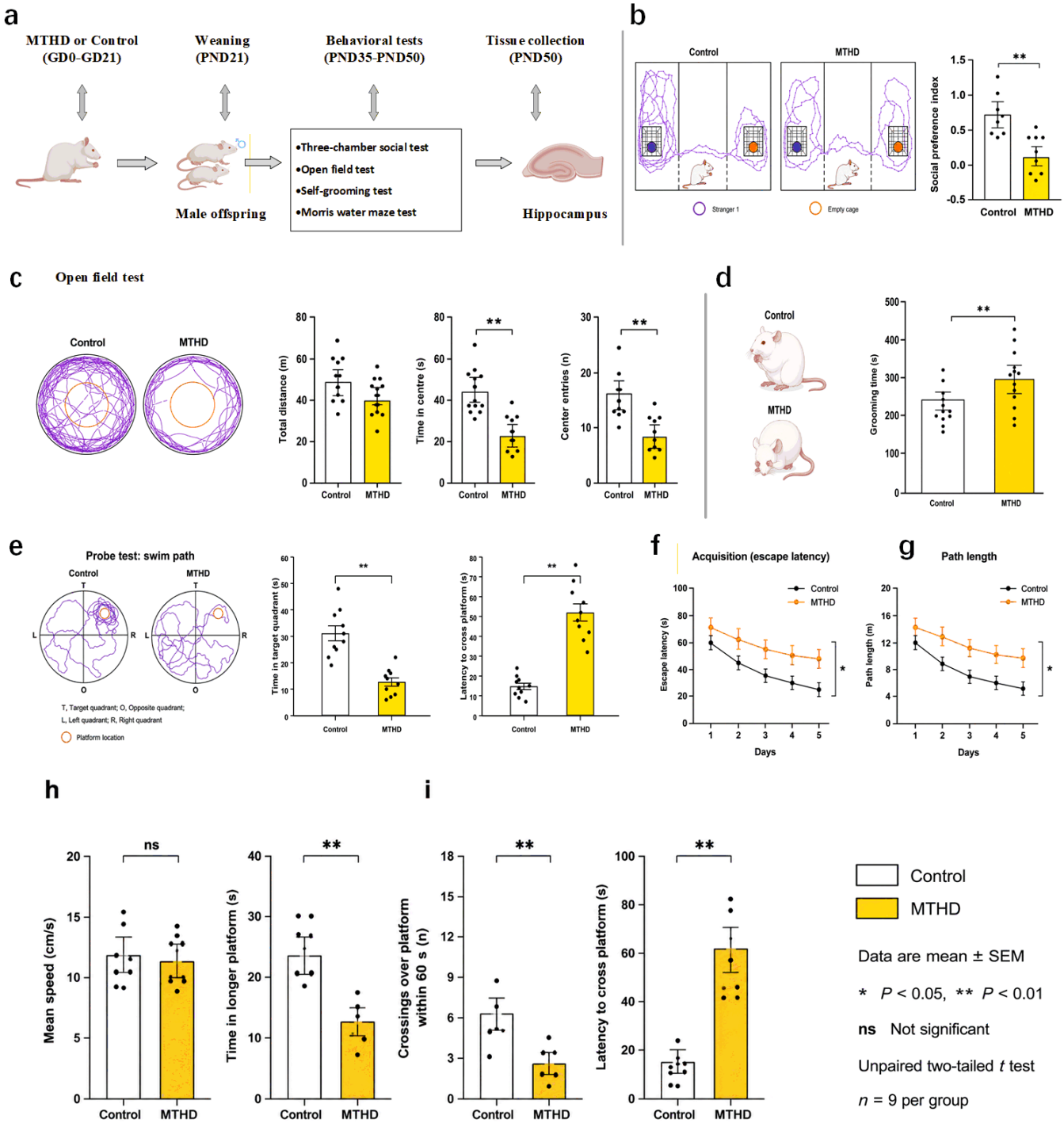


Figure 1

Maternal thyroid hormone deficiency induces neurodevelopmental behavioral abnormalities in offspring. (a) Experimental workflow showing maternal thyroid hormone deficiency (MTHD) or control exposure from gestational day 0 (GD0) to GD21, weaning at PND21, behavioral testing during PND35-PND50, and hippocampal tissue collection at PND50. (b) Representative movement traces and

quantification from the three-chamber social test showing reduced social preference in MTHD offspring. (c) Representative open-field movement traces and quantification of total distance, time in the center zone, and center entries. (d) Representative self-grooming behavior and quantification of grooming time. (e) Representative Morris water maze probe-trial swim paths and quantification of time in the target quadrant and escape-passage latency. (f) Escape latency during Morris water maze acquisition training. (g) Path length during Morris water maze acquisition training. (h) Probe-trial mean swim speed and time in the former platform quadrant. (i) Probe-trial platform crossings within 60 s and latency to cross the former platform location. Data are presented as mean ± SEM, n = 9 biologically independent male offspring from 9 independent litters per group. Between-group comparisons were performed using an unpaired two-tailed Student's t-test; acquisition training in the Morris water maze was analyzed using two-way repeated-measures ANOVA followed by Bonferroni post hoc correction. ns, not significant; *P < 0.05, **P < 0.01.

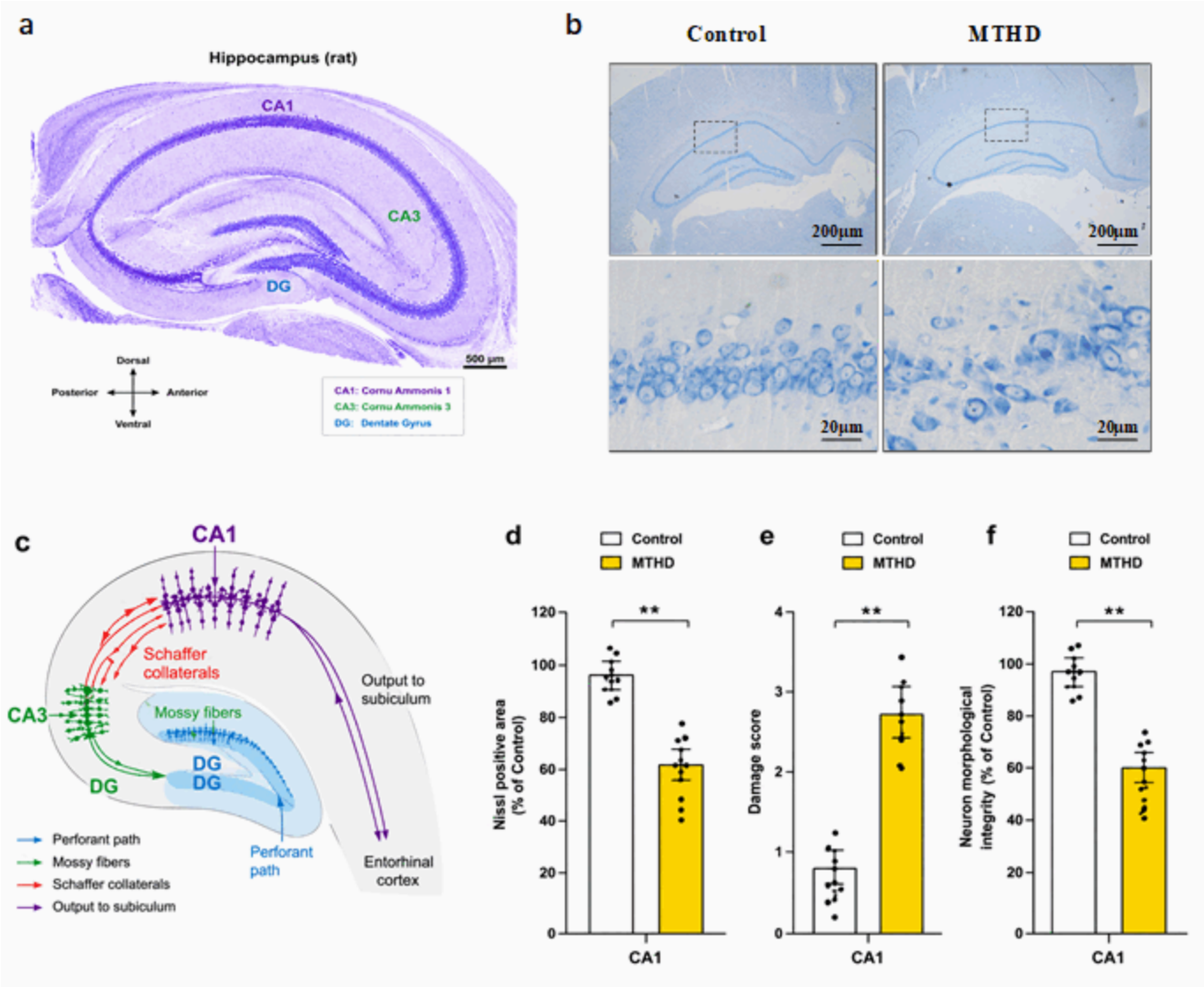


Figure 2

Maternal thyroid hormone deficiency impairs neuronal cytoarchitecture in the hippocampal CA1 region of offspring. (a) Schematic coronal anatomy of the adult rat hippocampus showing the major hippocampal subregions, including CA1, CA3 and the dentate gyrus (DG). (b) Representative Nissl-stained images of the hippocampal CA1 region in Control and MTHD offspring. (c) Schematic of the hippocampal CA1 neural circuit, illustrating inputs from CA3 Schaffer collaterals and perforant-path projections from the entorhinal cortex, and output projections to the subiculum. (d) Quantification of the Nissl-positive area in the CA1 region. (e) Quantification of the tissue injury score in the CA1 region. (f) Quantification of neuronal morphological integrity in the CA1 region. Data are presented as mean ± SEM, n = 9 biologically independent male offspring from 9 independent litters per group. Between-group comparisons were performed using an unpaired two-tailed Student's t-test. $^{**}P < 0.01$.

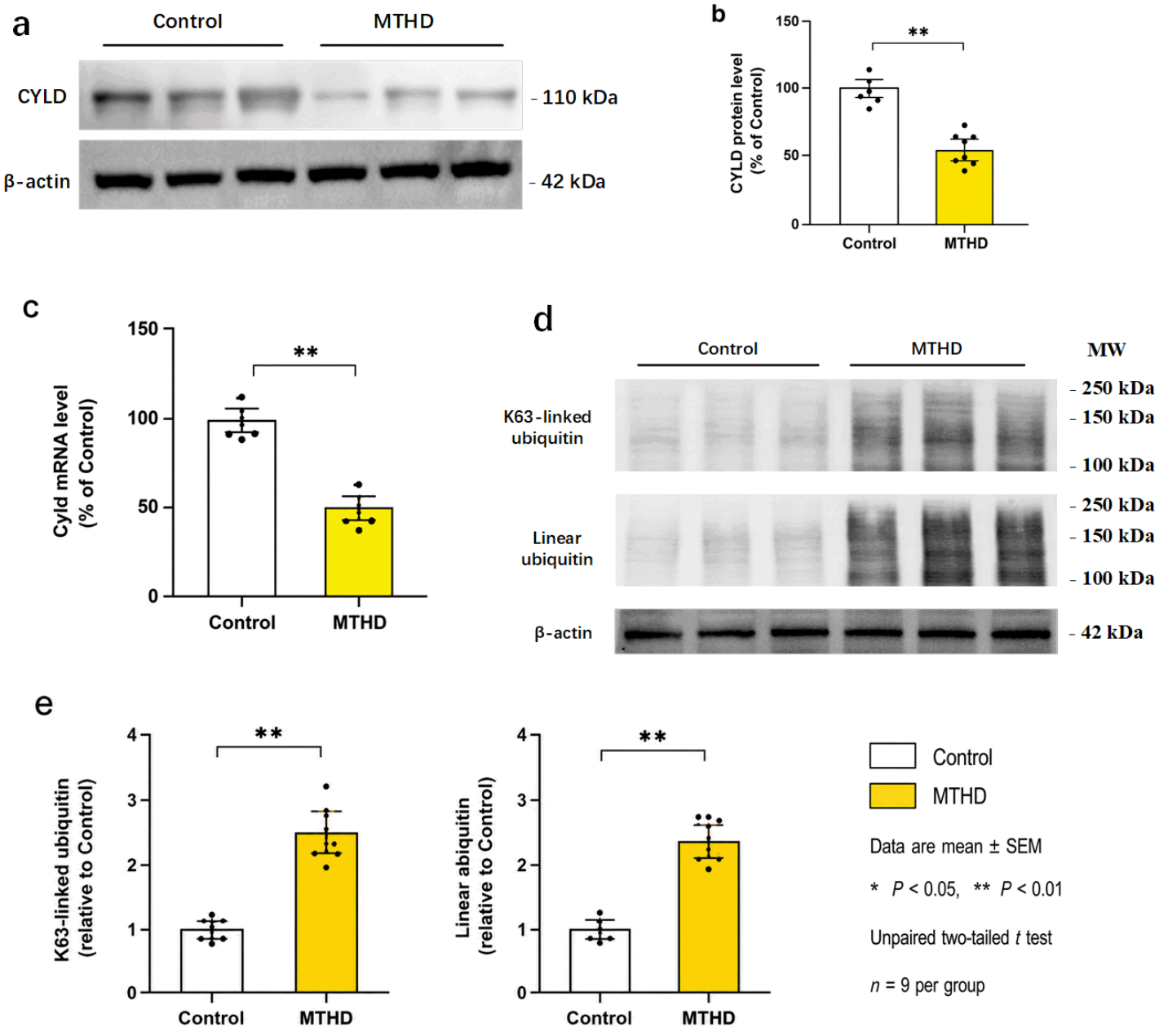


Figure 3

Maternal thyroid hormone deficiency disrupts CYLD-associated ubiquitin homeostasis in the hippocampus. (a) Representative Western blots showing hippocampal CYLD protein expression in Control and MTHD offspring. (b) Quantification of hippocampal CYLD protein expression. (c) RT-qPCR analysis of Cyld mRNA expression. (d) Western blot analysis and quantification of K63-linked ubiquitin signals in the high-molecular-weight region. (e) Western blot analysis and quantification of linear/Met1-linked ubiquitin signals in the high-molecular-weight region. Data are presented as mean ± SEM, n = 9 biologically independent male offspring from 9 independent litters per group. Between-group comparisons were performed using an unpaired two-tailed Student's t-test. ***P* < 0.01.

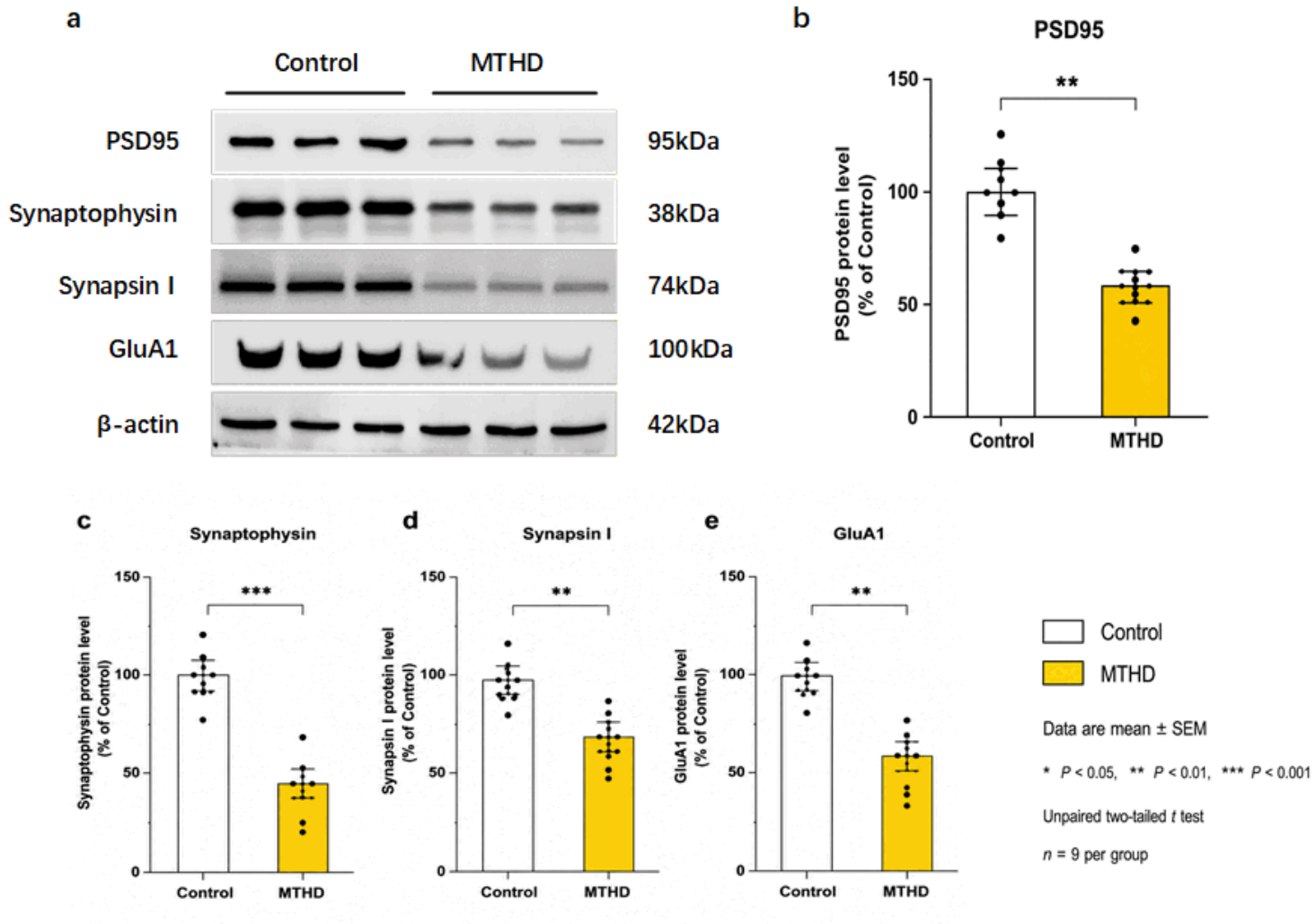


Figure 4

Maternal thyroid hormone deficiency disrupts hippocampal synaptic protein homeostasis. (a) Representative Western blots showing hippocampal expression of the synapse-associated proteins PSD95, synaptophysin, Synapsin I and GluA1. (b) Quantification of PSD95 protein expression. (c) Quantification of synaptophysin protein expression. (d) Quantification of Synapsin I protein expression. (e) Quantification of GluA1 protein expression. Data are presented as mean ± SEM, n = 9 biologically independent male offspring from 9 independent litters per group. Between-group comparisons were performed using an unpaired two-tailed Student's t-test. ***P* < 0.01, ****P* < 0.001.

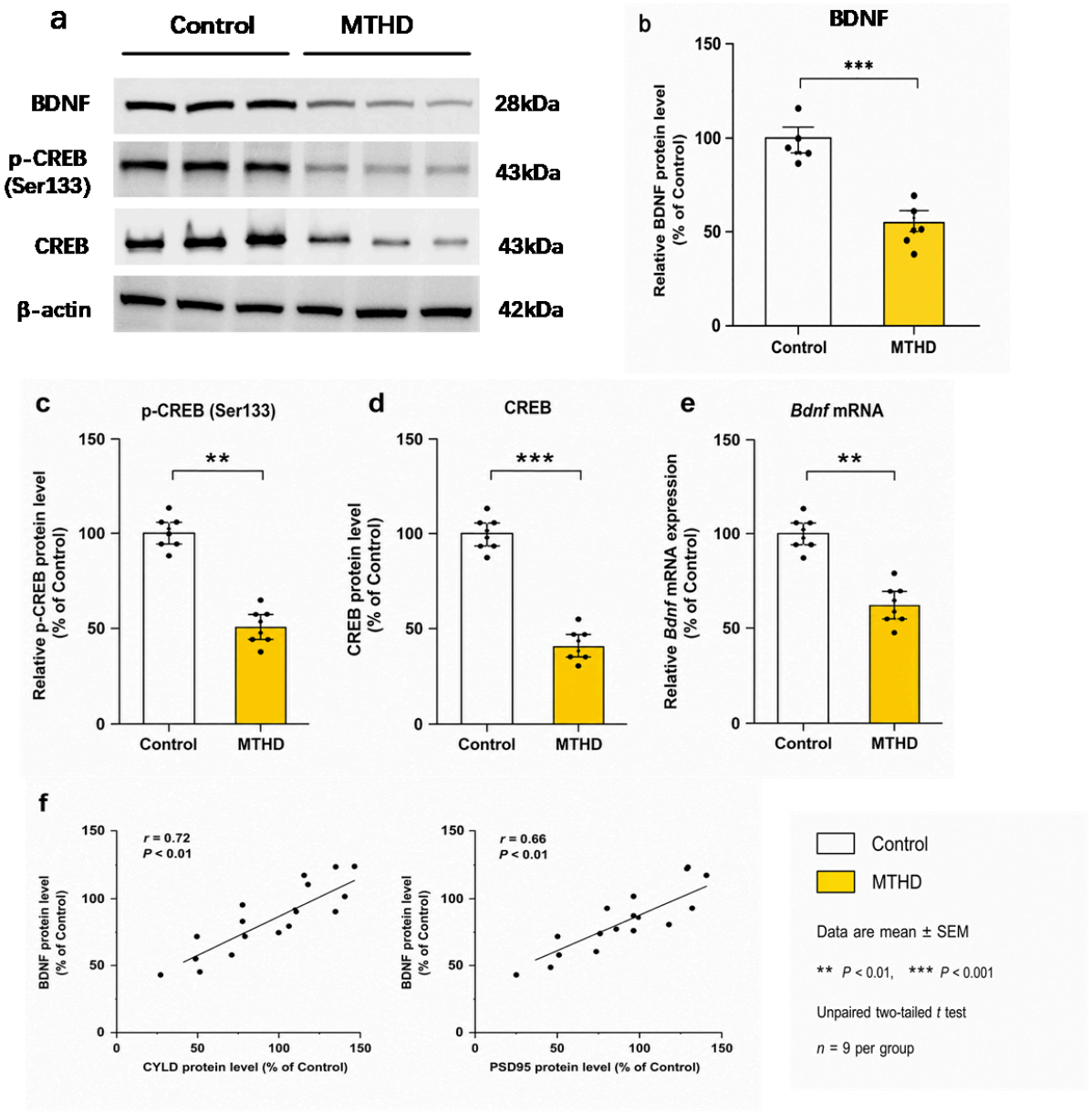


Figure 5

Maternal thyroid hormone deficiency suppresses hippocampal BDNF-CREB neurotrophic signaling. (a) Representative Western blots showing hippocampal expression of BDNF, phosphorylated CREB at Ser133 [p-CREB (Ser133)] and total CREB. (b) Quantification of BDNF protein expression. (c) Quantification of p-CREB (Ser133) protein expression. (d) Quantification of total CREB protein expression. (e) RT-qPCR analysis of Bdnf mRNA expression. (f) Pearson correlation analyses showing the relationships between BDNF protein expression and CYLD protein expression, and between BDNF protein expression and PSD95 protein expression. Data are presented as mean ± SEM, n = 9 biologically independent male offspring from 9 independent litters per group. Between-group comparisons were performed using an unpaired two-tailed Student's t-test; correlations were assessed using Pearson correlation analysis. $^{**}P < 0.01$, $^{***}P < 0.001$.

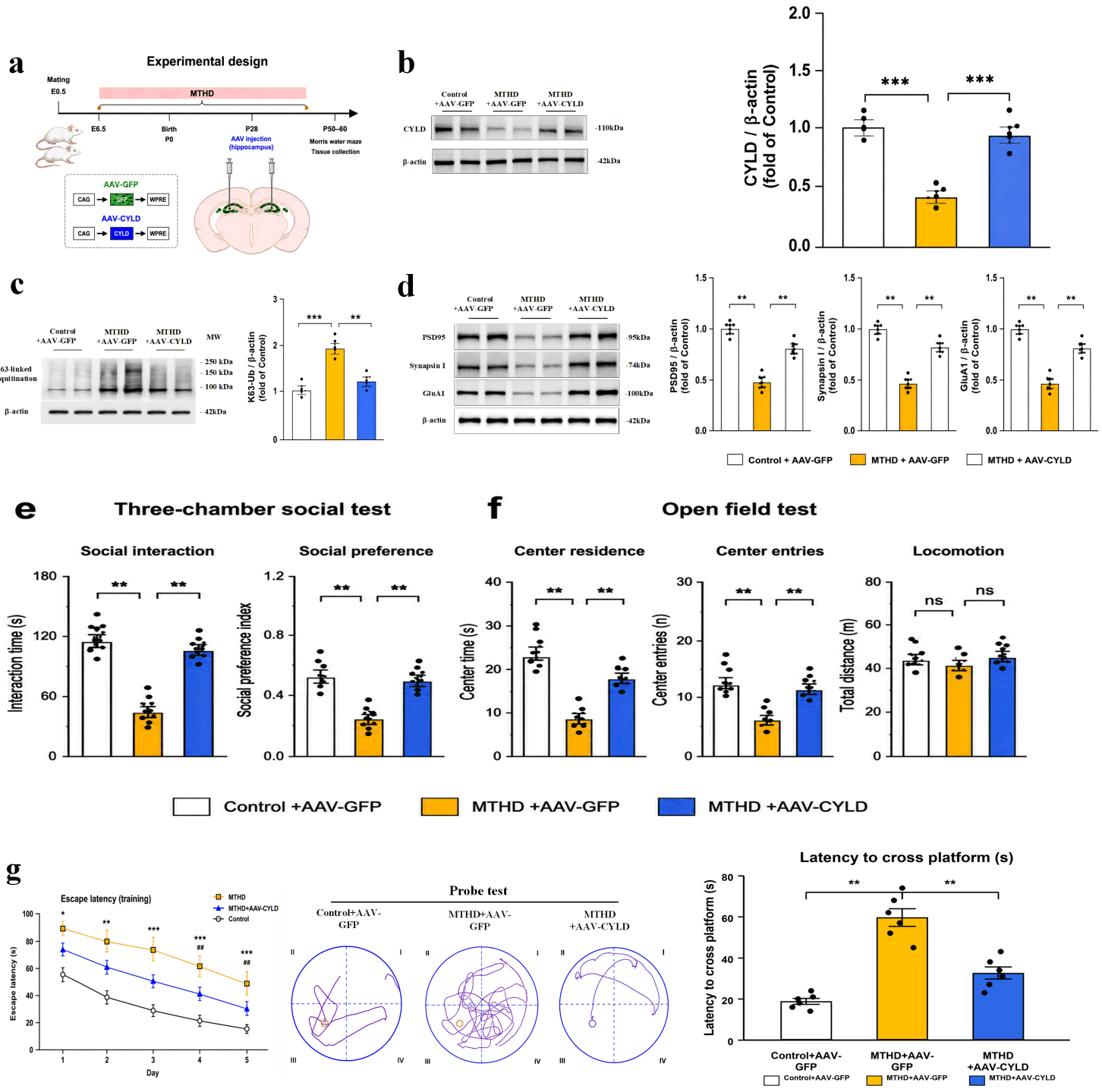


Figure 6

Postnatal hippocampal CYLD overexpression attenuates K63-linked ubiquitin accumulation and improves synaptic and behavioral outcomes in MTHD offspring. (a) Schematic of the AAV-mediated hippocampal CYLD overexpression experiment. Male offspring received bilateral stereotaxic hippocampal injections of AAV-GFP or AAV-CYLD at postnatal day 28 (P28), followed by behavioral testing at P50-P60 and hippocampal tissue collection for molecular analyses. (b) Representative Western blots and quantification of hippocampal CYLD protein expression. (c) Representative Western

blots and quantification of K63-linked ubiquitin signals in the high-molecular-weight region. (d) Representative Western blots and quantification of synapse-associated proteins, including PSD95, Synapsin I, and GluA1. (e) Quantification of social interaction time and social preference index in the three-chamber social test. (f) Quantification of center-zone residence time, center entries, rearing behavior, and total locomotor distance in the open field test. (g) Morris water maze analysis, including escape latency during acquisition training, representative probe-trial swim paths, and latency to cross the former platform location. Data are presented as mean ± SEM. Sample sizes are indicated by individual data points in each graph; each point represents one biologically independent male offspring from an independent litter. For Western blot analyses, representative blots are shown, and densitometric quantification was performed using independent biological samples. Escape latency during acquisition training was analyzed using two-way repeated-measures ANOVA followed by Bonferroni post hoc correction; other comparisons were analyzed using one-way ANOVA followed by Tukey's multiple-comparisons test. ns, not significant; *P < 0.05, **P < 0.01, ***P < 0.001.

Supplementary Files

This is a list of supplementary files associated with this preprint. Click to download.

- SupplementaryTables.docx
- fulluncroppedGelsandBlotsimages.docx